



## 10 SUPPLEMENTARY INFORMATION TEXT

11

### 12 Phase-retrieval holographic reconstruction

13 Figure S4 presents a scheme of our lens-free in-line holography configuration and introduces  
14 the notations represents. An incident plane wave  $U_{inc}$  illuminates an object with complex  
15 transmission  $\alpha_0$ , located at plane  $z=0$ . The complex amplitude in the plane right after the  
16 object is expressed as:

$$17 \quad A_0 = U_{inc} \cdot \alpha_0 \quad (1)$$

18 In the sensor plane located at plane  $z = Z$ , the complex amplitude  $A_Z$  results from the  
19 convolution of the complex amplitude in the object plane  $A_0$  with the Fresnel propagation  
20 function  $h_Z$

$$21 \quad A_Z = A_0 * h_Z = U_{inc} \cdot \alpha_0 * h_Z = U_{inc} \cdot \alpha_Z \quad (2)$$

$$22 \quad h_Z(r) = \frac{1}{j\lambda Z} \exp(jkZ) \exp\left(j \frac{\pi r^2}{\lambda Z}\right) \quad (3)$$

23 where  $k = 2\pi/\lambda$  is the wave number and  $j$  is the unit imaginary number such that  $j^2 = -1$ .

24 We define  $\alpha_Z$  the normalized complex amplitude in the sensor plane, as:

$$25 \quad \alpha_Z = m_Z \exp(j\phi_Z) \quad (4)$$

26 where  $\phi_Z = \text{Arg}(\alpha_Z)$  is the phase and  $m_Z$  is the modulus of  $\alpha_Z$ .

27 The intensity  $I_Z$  is recorded by the sensor without any phase information:

28  $I_Z = |A_Z|^2 = |U_{inc}|^2 \cdot |\alpha_Z|^2$  (5)

29  $|U_{inc}|^2$  is the background intensity that is recorded when there is no object above the sensor.

30 Note that without object,  $\alpha_0 = 1$  and consequently  $I_Z = |U_{inc}|^2$ . The modulus  $m_Z$  is  
 31 obtained through the measurement of  $I_Z$ :

32  $m_Z = |\alpha_Z| = \sqrt{\frac{I_Z}{|U_{inc}|^2}}$  (6)

33 The purpose of the holographic reconstruction algorithm is to recover the complex image of  
 34 the sample  $\alpha_0$  from the phase-less recorded holographic image  $m_Z$  [11]. We have developed  
 35 an algorithm based on the formulation of the phase retrieval problem discussed in [19]. After  
 36 initialization, the algorithm refines the estimate of the complex image in the sensor plane by  
 37 iteratively applying update rules in a gradient descent. (Step 1) of our phase retrieval  
 38 algorithm consists in the initialization of the complex amplitude in the sensor plane  $\alpha_Z$  by  
 39 setting its phase to zero:  $\phi_Z = 0$ . (Step 2) consists in back-propagating the complex  
 40 amplitudes to the object plane, using the inverse Fresnel function (Eq. 3):

41  $\alpha_0 = \alpha_Z * h_{-Z} = m_Z * h_{-Z}$  (7)

42 Fig. S5 shows as an example the module and the phase of  $\alpha_0$  after a single back-propagation  
 43 of lensfree acquisition of a CSF specimen. At this stage the complex image is impaired by the  
 44 presence of an artefact, the so-called “twin image” that results from a lack of phase  
 45 information during the acquisition process. In (Step 3) we define a cost function  $\varepsilon(\alpha_0)$  to be  
 46 minimized in order to reduce the “twin image” artefact. Here in the case of CSF sample, we  
 47 used the total variation norm:

$$48 \quad \varepsilon(\alpha_0) = \iint dx.dy. \sqrt{\left| \frac{\partial \alpha_0(x, y)}{\partial x} \right|^2 + \left| \frac{\partial \alpha_0(x, y)}{\partial y} \right|^2} \quad (8)$$

49 This cost function is minimized when the objects are locally uniform and sparsely distributed  
50 which is verified in the case of CSF sample. As the signals are discrete, the derivative  
51 operators are replaced by Sobel operators ( $S_x, S_y$ ) and the integrals by sums. The cost  
52 function rewritten as a function of the unknown  $\varphi_z$  of the problem becomes:

$$53 \quad \varepsilon(\varphi_z) = \sum_{i,j} \sqrt{(S_x * \alpha_0(\varphi_z))_{ij} \cdot (S_x * \alpha_0(\varphi_z))_{ij}^* + (S_y * \alpha_0(\varphi_z))_{ij} \cdot (S_y * \alpha_0(\varphi_z))_{ij}^*}$$

$$S_x = \begin{bmatrix} 1 & 0 & -1 \\ 2 & 0 & -2 \\ 1 & 0 & -1 \end{bmatrix}, S_y = \begin{bmatrix} 1 & 2 & 1 \\ 0 & 0 & 0 \\ -1 & -2 & -1 \end{bmatrix} \quad (9)$$

$$\alpha_0(\varphi_z) = \left( m_z e^{i\varphi_z} \right) * h_{-z}$$

54 where  $i$  and  $j$  are the indices of pixels. In the following (Step 4) the unknown  $\varphi_z$  is  
55 iteratively refined according to a conjugated gradient scheme:

$$56 \quad \varphi_z^{(k)} = \varphi_z^{(k-1)} + s^{(k)} \cdot p^{(k)} \quad (10)$$

57 where  $p^{(k)}$  is the direction of the descent (with the same dimensions as  $\varphi_z$ ) and  $s^{(k)}$  is a  
58 scalar which gives the step length in the direction of descent. In Eq. (10), the choice of the  
59 direction of descent  $p^{(k)}$  is given as a function of the gradient of the cost function  $\varepsilon(\varphi)$  and  
60 the direction obtained at the previous iteration :

$$61 \quad p^{(k)} = -\nabla \varepsilon + \beta p^{(k-1)} \quad (11)$$

62 with  $p^{(-1)} = 0$  and  $\beta$  a scalar defined according to e.g. the Fletcher-Reeves method :

$$\beta^{(k)} = \frac{\nabla \varepsilon^{(k)} \cdot \nabla \varepsilon^{(k)}}{\nabla \varepsilon^{(k-1)} \cdot \nabla \varepsilon^{(k-1)}} \quad (12)$$

64 The gradient of the cost function, e.g. the variation of the cost function for every variation in  
65  $\varphi_z$  is obtained analytically from Eq. 9 :

$$\nabla \varepsilon = \frac{\partial \varepsilon}{\partial \varphi Z} = \text{Im } A_z^* \left( \left( S_x * \frac{S_x * A_0}{\sqrt{|S_x * A_0|^2 + |S_y * A_0|^2}} + S_y * \frac{S_y * A_0}{\sqrt{|S_x * A_0|^2 + |S_y * A_0|^2}} \right) * h_z \right)$$

67 (13)

68 In Eq. (10), the step length  $s^{(k)}$  is given by a minimization-majoration method [20] obtained  
69 by majoring the cost function  $\varepsilon(\varphi_z)$  (Eq. (9)) by a quadratic form:

$$s^{(k)} = - \frac{\text{Re} \sum_{ij} \left( X_{ij} \Delta X_{ij}^* + Y_{ij} \Delta Y_{ij}^* \right)}{\sum_{ij} \left( \Delta X_{ij} \Delta X_{ij}^* + \Delta Y_{ij} \Delta Y_{ij}^* \right)}$$

$$D_{ij} = \sqrt{\left( S_x * \alpha_0 \left( \varphi^{(k-1)} \right) \right)_{ij} \cdot \left( S_x * \alpha_0 \left( \varphi^{(k-1)} \right) \right)_{ij}^* + \left( S_y * \alpha_0 \left( \varphi^{(k-1)} \right) \right)_{ij} \cdot \left( S_y * \alpha_0 \left( \varphi^{(k-1)} \right) \right)_{ij}^*}$$

$$X_{ij} = \left( S_x * \alpha_0 \left( \varphi^{(k-1)} \right) \right)_{ij} / D_{ij}$$

$$Y_{ij} = \left( S_y * \alpha_0 \left( \varphi^{(k-1)} \right) \right)_{ij} / D_{ij}$$

$$\Delta X_{ij} = i \left( S_x * p A_z \left( \varphi^{(k-1)} \right) * h_{-z} \right)_{ij} / D_{ij}$$

$$\Delta Y_{ij} = i \left( S_y * p A_z \left( \varphi^{(k-1)} \right) * h_{-z} \right)_{ij} / D_{ij}$$

71 (14)

72 (Step 4) is repeated typically 30 times to obtain the convergence of our algorithm.

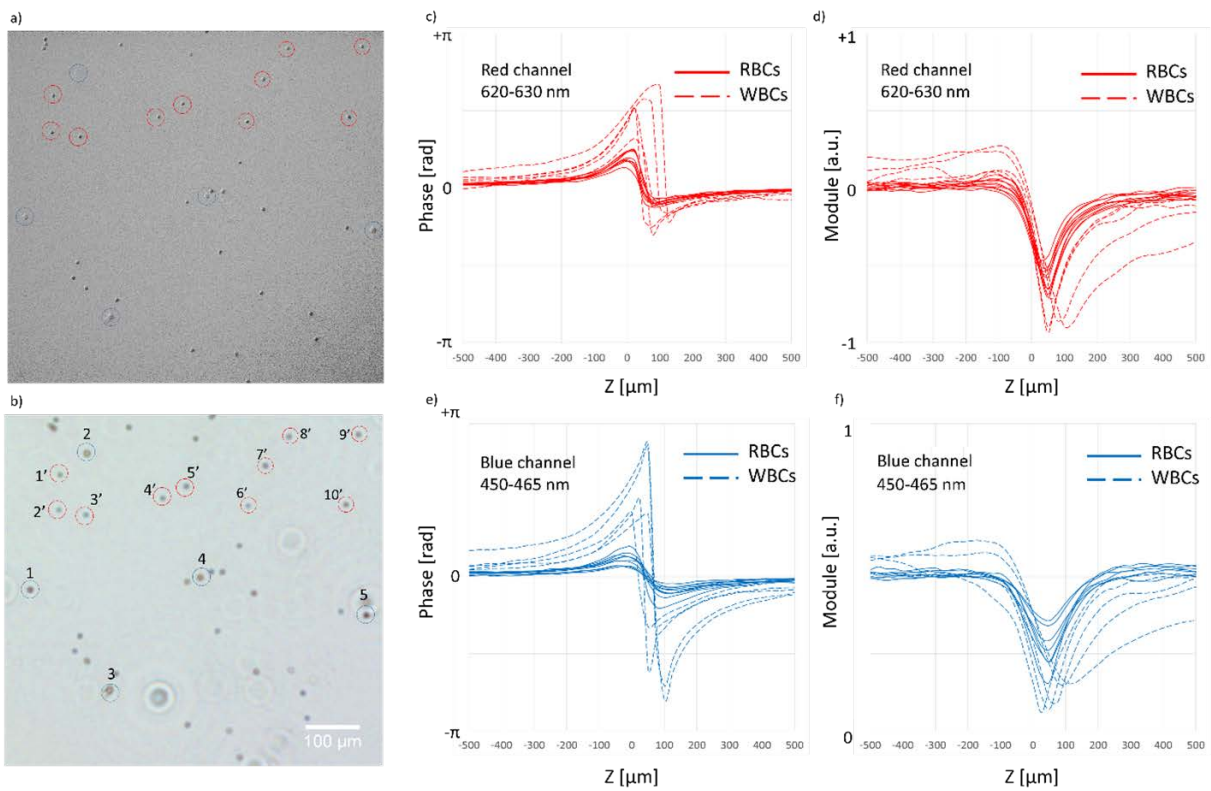
73 Measurement consistency is ensured since module  $m_Z$  is kept unchanged all along the

74 iterative process (Eq. (9)). Finally, the reconstructed complex image  $\alpha_0$  is obtained by  
75 propagating the refined complex image  $\alpha_Z$  to the object plane (Fig. S5).

76

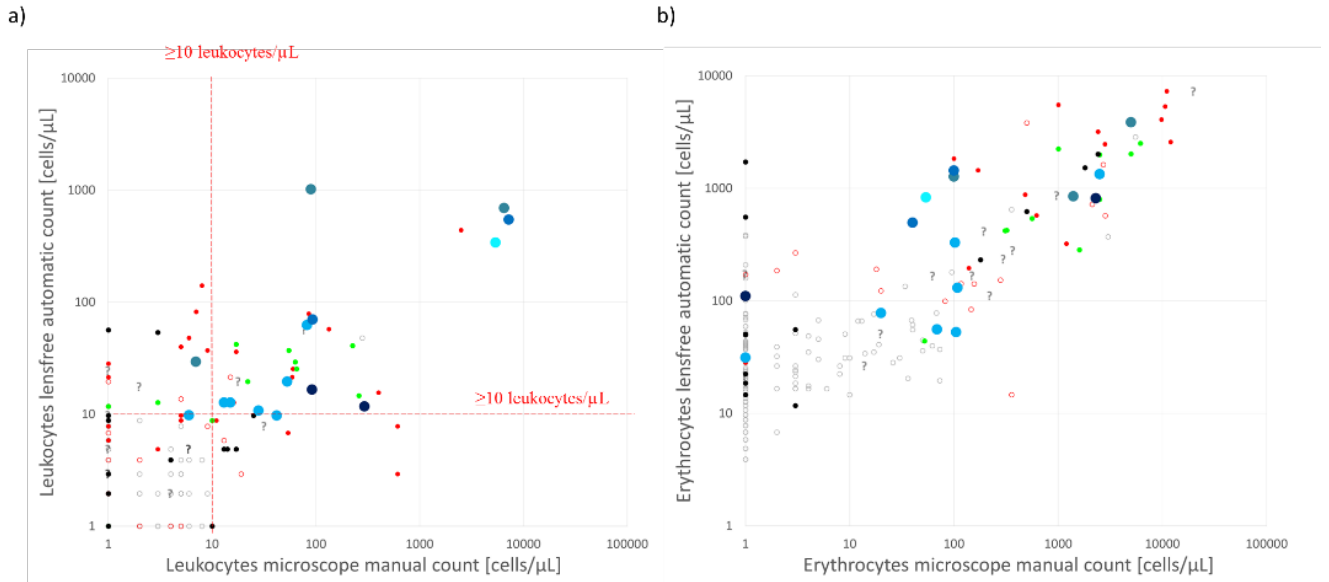
77 **SUPPLEMENTARY FIGURE LEGENDS**

78 **Figure S1.** Comparison between (a) the transmission image obtained with x10 magnification  
79 microscope and (b) the lensfree RGB reconstructed module image. Red and blue circles  
80 denote respectively erythrocytes (RBCs) and leukocytes (WBCs) as confirmed on (a) the  
81 microscope transmission image. The reconstructed (red channel) phase and module Z-axis  
82 profiles corresponding to the different cells circled in (a) are shown in (c) and (d)  
83 respectively. The leukocytes profiles are plotted with dotted lines and the erythrocytes profiles  
84 with plain line. The reconstructed phase and module Z-axis profiles (blue channel) are shown  
85 in (e) and (f) respectively.



86  
87

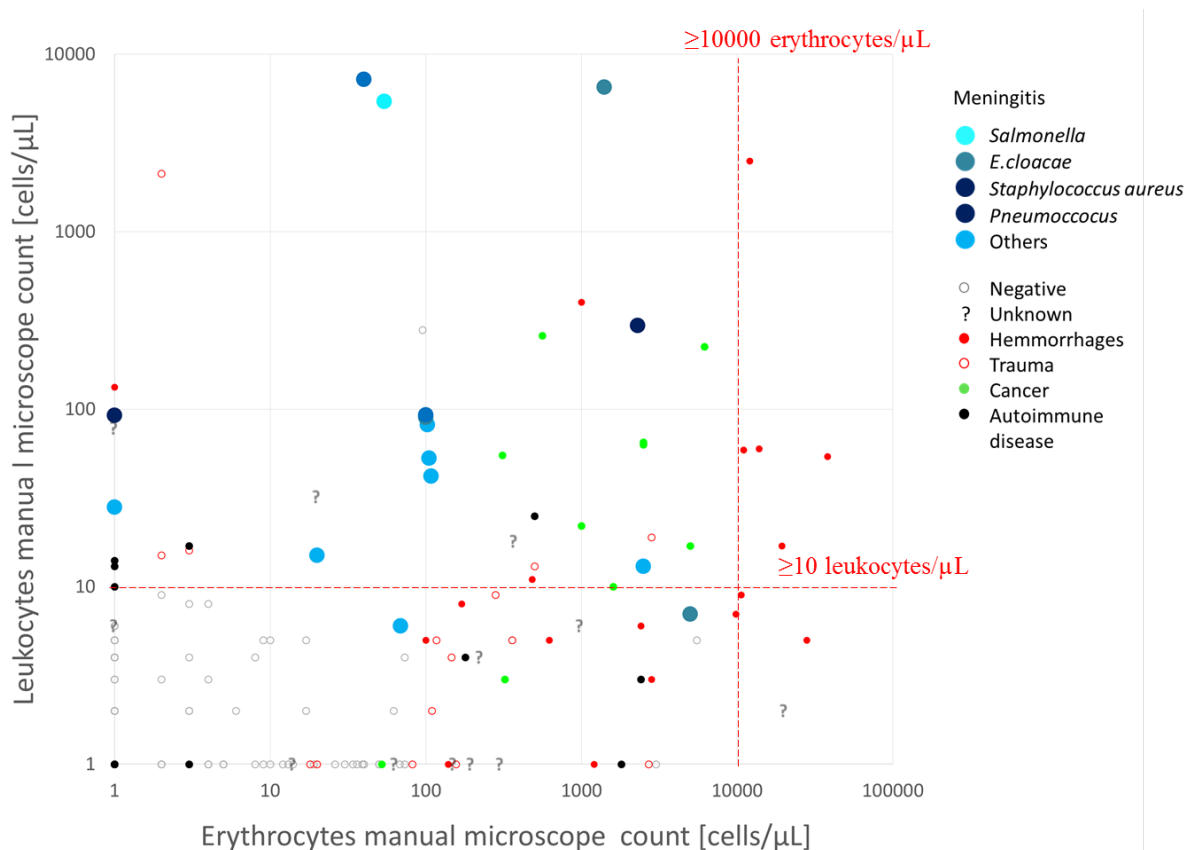
88 **Figure. S2.** Comparison between the lensfree automatic count and the reference optic  
89 microscopy counting for 215 cerebrospinal fluid clinical specimens (a) leukocytes counts (b)  
90 erythrocyte counts.



91  
92



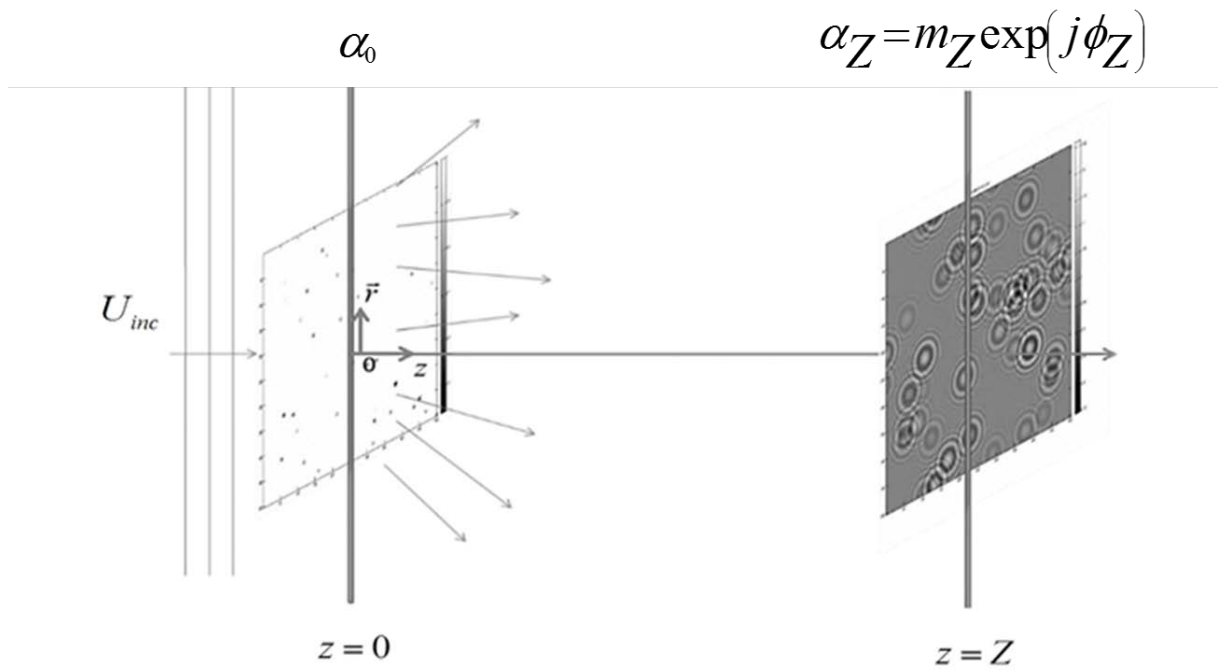
93 **Figure S3.** Scatterplot of the optic microscopy leukocyte and erythrocyte counts resulting  
 94 from the analysis of the first datasets featuring 215 clinical specimens. A color code has been  
 95 defined with respect to the different diagnosis established for all clinical specimens. The  
 96 infectious meningitis of interest are plotted in large blue dots. The limit of 10 cells/ $\mu\text{L}$  used  
 97 for the biological definition of meningitis is depicted by a horizontal red dotted line. The  
 98 obtained sensitivity is about 87% and the specificity is about 85%. There are two cases two  
 99 cases of infectious meningitis which have not been detected under microscope, the leukocytes  
 100 microscope count was respectively 6 and 7 leukocytes/ $\mu\text{L}$  well below the limit of 10 cells/ $\mu\text{L}$   
 101 used for the early diagnoses of meningitis. The specificity can be improved up to 87% if  
 102 additional criteria are applied to detect hemorrhagic samples in which the number of  
 103 erythrocyte is  $> 10.000$  cells/ $\mu\text{L}$ .



104

105

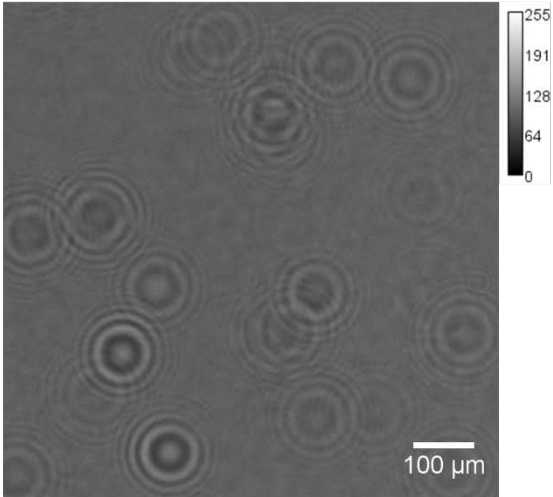
106 **Figure S4.** Principle of lens-free in-line holography. The object is located at  $z=0$ , the sensor is  
 107 at  $z=Z$ . Radial coordinates are defined by the vector  $\vec{r}$ . The object is illuminated by an  
 108 incident plane wave  $U_{inc}$ .  $\alpha_0$  is the normalized complex transmission of the object.  $\alpha_Z$  is  
 109 the normalized complex amplitude at the sensor plane.



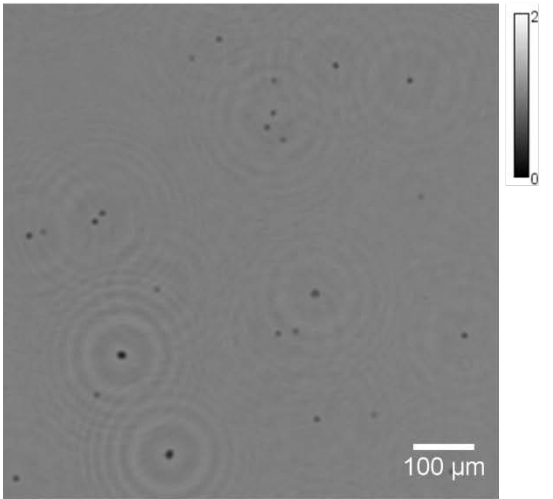
110  
 111

112 **Figure S5.** (a) Lensfree raw hologram acquired in the blue channel of the sample  
113 Q160550287 (ruptured brain aneurysm; microscope counting: 218 erythrocytes/ $\mu\text{L}$ , 14  
114 leukocytes/ $\mu\text{L}$ ). (b) Reconstructed module image after a single back-propagation. The image  
115 shows the presence of the so-called ‘twin image’, the cells are surrounded by concentric rings  
116 which result of lack of phase information. (c) Reconstructed module image obtained after 30  
117 iterations of the phase-retrieval algorithm. The phase in the sensor plane is well estimated and  
118 the reconstructed image is now free of ‘twin image’ (d) Reconstructed phase image after a  
119 single back-propagation. (e) Reconstructed phase image obtained after 30 iterations of the  
120 phase-retrieval algorithm. All images are cropped area of  $0.65\mu\text{m}^2$  out of the full field of view  
121 of  $29.4\text{mm}^2$ .

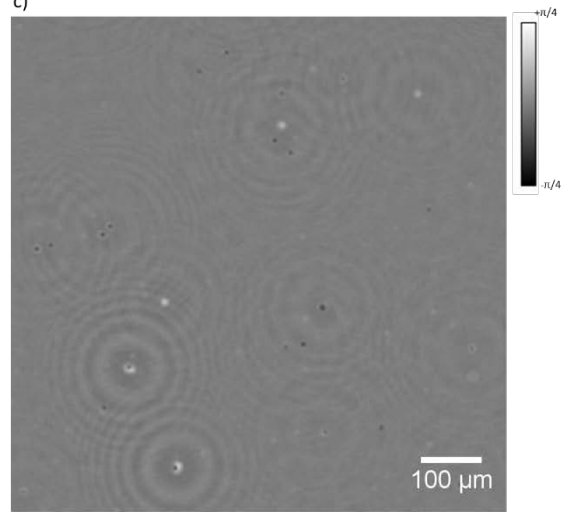
a)



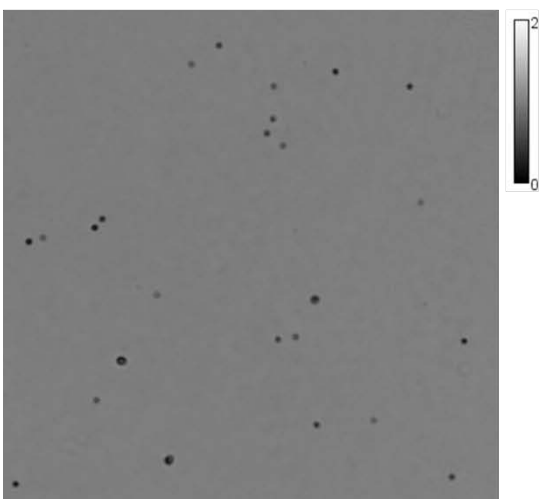
b)



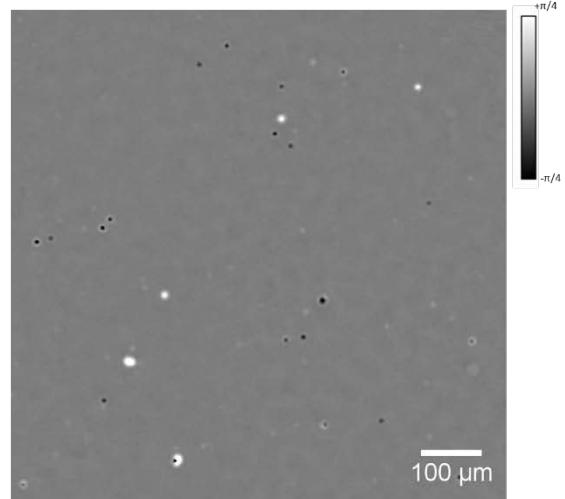
c)



d)



e)



123 **Figure S6.** (a) Cell classification performed on the module reconstructed image (red channel)  
124 of the sample Q150430694 (autoimmune disease; microscope counting: 1800  
125 erythrocytes/ $\mu\text{L}$ , 0 leukocytes/ $\mu\text{L}$ ) over a cropped area of  $11.6\mu\text{m}^2$ . Red circles denote the  
126 detection of the erythrocytes, black circles denote the detection of small particles or false  
127 detections, and blue circles denote objects with large phase amplitude which are likely  
128 leukocytes (b) Detail of (a) (yellow rectangle).

